Biomedicine & Pharmacotherapy 141 (2021) 111681

Contents lists available at ScienceDirect

Biomedicine & Pharmacotherapy

journal homepage: www.elsevier.com/locate/biopha

Anti-neoplastic and demethylating activity of a newly synthetized flavanone-derived compound in Renal Cell Carcinoma cell lines

A.Ângela Marques-Magalhães [a,b], Inês Graça [a], Vera Miranda-Gonçalves [a], Rui Henrique [a,c,d], Marie Lopez [e], Paola B. Arimondo [f], Carmen Jerónimo [a,d,*]

[a] Cancer Biology and Epigenetics Group, IPO Porto Research Center (CI-IPOP), Portuguese Oncology Institute of Porto (IPO Porto), Porto 4200-072, Portugal
[b] Institute of Biomedical Sciences Abel Salazar, University of Porto (ICBAS-UP), Rua Jorge Viterbo Ferreira 228, 4050-513 Porto, Portugal
[c] Department of Pathology, Portuguese Oncology Institute of Porto (IPO Porto), Porto 4200-072, Portugal
[d] Department of Pathology and Molecular Immunology, Institute of Biomedical Sciences Abel Salazar (ICBAS), University of Porto, Porto 4050-313, Portugal
[e] Institut des Biomolécules Max Mousseron (IBMM), CNRS, Université de Montpellier, ENSCM UMR 5247, Montpellier 34296, France
[f] Epigenetic Chemical Biology, Institut Pasteur, CNRS UMR3523, Paris 75724, France

ARTICLE INFO

Keywords:
Renal Cell Carcinoma
DNA methylation
3-nitroflavanones
DNMT inhibitors
Anticancer therapy

ABSTRACT

Renal Cell Carcinoma (RCC) is on the top 10 of the most incident cancers worldwide, being a third of patients diagnosed with advanced disease, for which no curative therapies are currently available. Thus, new effective therapeutic strategies are urgently needed. Herein, we tested the antineoplastic effect of newly synthesized 3-nitroflavanones (MLo1302) on RCC cell lines. 786-O, Caki2, and ACHN cell lines were cultured and treated with newly synthesized 3-nitroflavanones. IC50 values were calculated based on the effect on cell viability assessed by MTT assay, after 72 h of exposure. MLo1302 displayed antineoplastic properties in RCC cell lines through marked reduction of cell viability, increased apoptosis and DNA damage, and morphometric alterations indicating a less aggressive phenotype. MLo1302 induced a significant reduction of global DNA methylation and DNMT mRNA levels, increasing global DNA hydroxymethylation and TET expression. Moreover, MLo1302 decreased DNMT3A activity in RCC cell lines, demethylated and re-expressed hypermethylated genes in CAM-generated tumors. A marked *in vivo* decrease in tumor growth and angiogenesis was also disclosed. MLo1302 disclosed antineoplastic and demethylating activity in RCC cell lines, constituting a potential therapeutic agent for RCC patients.

1. Introduction

Renal cell carcinoma (RCC) is the most frequent kidney cancer type (≈85%) with a male to female ratio of 2.0:1.0, representing the 7th and 10th most common cancer in men and women, respectively, and steadily increasing over the last decades [1,2]. Clear cell RCC (ccRCC) is the most frequent RCC histological subtype (≈ 80%) followed by papillary (pRCC) and chromophobe RCC (chRCC), which represents 80% of the non-ccRCC [3]. RCC represents a heavy economic burden on the healthcare system due to the high morbidity and mortality rate. Despite the curative intent of nephrectomy, about 30% of RCC cases are diagnosed with locally advanced disease and distant metastases. At these stages, therapy regimens with tyrosine kinase inhibitors allow for disease control, increasing median survival for up to 9 months. Nonetheless, this treatment is not curative and eventually all metastatic RCC (mRCC) patients will develop resistance, disclosing a 5-year survival rate inferior to 10% [4,5]. Thus, considering RCC biology, it is imperative to improve not only early detection approaches but also new and more effective therapeutic strategies for locally advanced and metastatic disease. Importantly, several tumor suppressor genes (TSGs) involved in critical pathways for cellular homeostasis maintenance were found silenced by promoter methylation in RCC [6–9]. Indeed, TSG hypermethylation has been reported in about 20% and 7% of ccRCC and pRCC, respectively [10,11]. Specifically, *MTHFR* (ccRCC: 100%; pRCC: 100%), *RASSF1A* (ccRCC: 81%; pRCC: 100%), and *TIMP3* (≈ 58%) were shown to be highly methylated in RCC [6,8]. Taking advantage of the reversible nature of epigenetic modifications, modulation of epigenetic machinery using inhibitors of the DNMT, the DNA methyltransferases, might provide new and more effective therapeutic strategies for cancer, including RCC [12,13].

* Correspondence to: Portuguese Oncology Institute of Porto (IPOP), R. Dr. António Bernardino de Almeida, Porto 4200-072, Portugal.
E-mail addresses: carmenjeronimo@ipoporto.min-saude.pt, cljeronimo@icbas.up.pt (C. Jerónimo).

https://doi.org/10.1016/j.biopha.2021.111681
Received 4 March 2021; Received in revised form 20 April 2021; Accepted 28 April 2021
Available online 15 June 2021

Over the last decades, several compounds were tested in an attempt to restore the normal methylation patterns through inhibition of DNMTs [14,15], triggering their proteasomal degradation [16,17]. This strategy might contribute to the reversion of cancer cell phenotype and improvement of patient outcome [18]. Indeed, the clinical benefit of DNMT inhibitors (DNMTi) in hematologic cancer patients observed in clinical trials [19,20] led to U.S. Food and Drug Administration (FDA) and European Medicines Agency (EMA) approvals of 5-azacytidine and 5-aza-2'-deoxycytidine for treatment of myelodysplastic syndrome, acute myelomonocytic leukemia and chronic myelomonocytic leukemia [21,22]. However, these drugs display several limitations, including neutropenia and thrombocytopenia at higher doses due to cytotoxic effects [23], physiological instability, and short half-life due to the degradation by hydrolytic cleavage and deamination by cytidine deaminase [24,25]. Moreover, the lack of specificity might lead to aberrant expression of normally silenced genes, contributing to tumorigenesis [26]. Although other cytidine analogs with improved stability and efficacy have been developed, the cytotoxic effects inherent to nucleoside analogs, derived from their incorporation into DNA [27], entailed the development of new compounds that inhibit DNA methylation without requiring DNA incorporation [28]. Notably, natural products, including isothiocyanates (*e.g.* phenethyl isothiocyanate), polyphenols (*e.g.* epigallocatechin-3-gallate (EGCG), genistein, curcumin) and flavonoids (*e.g.* flavanones), present in food, constitute a class of compounds with antioxidant and anti-tumor properties that affect the epigenome, including alterations on DNA methylation [29,30]. These compounds also induce apoptosis, inhibit cancer cell proliferation, invasion and migration by affecting several important signaling pathways [31]. These natural products are widely available in dietary and disclosed low toxicity and good tolerability [31,32]. Among them, flavanones are a subgroup of flavonoids abundantly found in plants such as tea and citrus fruits [33]. Despite their potential clinical utility, natural compounds and their derivatives have not been extensively explored in urological cancer. Hence, we sought to explore the anti-neoplastic activity of newly synthetized 3-nitroflavanones [34] in RCC, dissecting the underling molecular mechanisms and focusing in its expected demethylating action.

2. Materials and methods

2.1. Chemicals

3-Nitroflavanones DD880, MLo1302, MLo1507, MLo1508 and MLo1607 were synthetized as described in [34] as compounds Flv880, 1, 3, 4 and 19, respectively. Stock solution of 10 mM DMSO were prepared, aliquoted and kept at − 20 °C. Two different batches were prepared and used in the experiments.

2.2. Cell culture and drug administration

Four ATCC epithelial renal cell lines (Lockville, MD, USA) available at our laboratory [HKC8 (benign kidney cell line), 786-O (primary ccRCC), Caki-2 (primary pRCC) and ACHN (metastatic pRCC)] were cultured in the recommended medium supplemented with 10% Fetal Bovine Serum (FBS) (Merck, Berlin, Germany) and 1% Antibiotic-Antimycotic (Anti-Anti (100x), GIBCO, Waltham, MA, USA), and were maintained at 37 °C in a humidified atmosphere containing 5% CO_2. All cell lines were routinely tested for *Mycoplasma* spp. contamination (PCR Mycoplasma Detection Set, Takara Bio, Shiga, Japan). Five recently characterized 3-nitroflavanones [34] were dissolved with dimethyl sulfoxide (DMSO, Sigma-Aldrich Corp., St. Louis, MO, USA) at 10 mM concentration and stored at − 20 °C until further use. Treatment was performed every 24 h during three consecutive days. For control purposes, cell lines were also exposed to the drug vehicle (DMSO).

2.3. Viability assay

Cell viability was evaluated using 3-(4,5-dimethylthiazol-2-yl)-2,5-diphenyltetrazolium-bromide (MTT) assay (Sigma-Aldrich). Cells were seeded onto 96-well plates at 1.5×10^4, 2×10^4, 3×10^4 and 2.5×10^4 cells per well for RWPE, 786-O, Caki-2 and ACHN, respectively. Cells were allowed to adhere overnight and then exposed to the IC50 and 2 × IC50 concentration of each compound or DMSO during three consecutive days, being the media renewed every 24 h. Afterwards, cell viability was measured at days 0, 1, 2 and 3. The absorbance was measured using a microplate reader (FLUOstar Omega, BMG Labtech, Offenburg, Germany) at 540 nm wavelength with background subtraction at 630 nm. Three replicates were used for each condition and at least three biological independent experiments were performed. The number of viable cells was calculated using the formula: [(experiment OD x number of cells at day 0)/Mean OD at day 0].

2.4. Apoptosis evaluation

Apoptosis was assessed using the APOPercentage™ apoptosis assay kit (Biocolor Ltd., Belfast, Northern Ireland), according to the manufacturer's guidelines. Briefly, 3×10^4 (786-O), 4×10^4 (Caki-2) and 3.5×10^4 (ACHN) cells/well were seeded onto 24-well plates, allowed to adhere overnight. After 72 h of compound exposure, 5% of the APOPercentage dye was added to the media and incubated at 37 ºC during 15–30 min, depending on cell type. After exposure to Dye Releasing Agent, absorbance was determined using a microplate reader (FLUOstar Omega) at 550 nm wavelength with background subtraction at 620 nm. Three biological and three experimental replicates were performed for each condition. Apoptosis levels were calculated according to the formula: [apoptosis OD/Mean MTT OD at day 3].

2.5. Single cell gel electrophoresis (comet assay)

Quantification of DNA fragmentation was evaluated as previously [35]. Briefly, after 72 h of drug exposure, 50,000 cells were harvested by trypsinization, washed in PBS and re-suspended in 75 μL of low-melting point agarose (Invitrogen, Carlsbad, CA, USA). This cell suspension was applied on top of a microscope slide containing normal-melting point agarose and allowed to polymerize for 20 min at 4 °C. The slides were then immersed in lysis solution, pH 10 (2.5 M NaCl, 100 mM Na_2EDTA, 10 mM Tris Base and Triton X-100 1%) at 4 °C during 2 h in the dark. Then, the slides were incubated in an alkaline electrophoresis buffer (300 mM NaOH, 1 mM Na_2EDTA, pH 13) for 40 min at 4 °C to allow DNA unwinding. Single cell gel electrophoresis was performed on a horizontal electrophoresis platform at 4 °C for 30 min at 27 V. The slides were then immersed in neutralization buffer (Tris–HCl; pH 7.5, 0.4 M Tris Base) for 10 min. After fixation with 100% ethanol, the slides were stained with Sybr Green® (Life Technologies, Foster City, CA, USA) and DNA damage was evaluated under a fluorescent microscope. At least three independent and two experimental replicates were performed for each condition. The DNA damaging effect through DNA fragmentation was determined by measuring four previously described parameters, including total intensity (DNA content), tail length, tail moment (a measure of both amount of DNA in the tail and its distribution) and percentage of DNA in the tail [36]. A minimum of 50 cells were considered for each of the three replicates.

2.6. Morphometric analysis

Cell morphometric analysis was performed after 72 h of exposure to the compound. Cell sphericity and area were evaluated using the free-hand polygon tool of the Olympus CellSens Dimension software (Olympus Corporation, Shinjuku, Japan). For each condition, at least 50 cells from the three biological replicates were analyzed.

2.7. Chicken chorioallantoic membrane (CAM) assay

Fertilized chicken eggs (Pintobar, Portugal) were incubated horizontally at 37 °C with 70% humidity (HERATHERM incubator; Thermo Scientific). At 3rd day of development, a small hole was shaped in the pointed end of the egg to allow CAM dissociation from the egg shell membrane and an oval window (≈ 2 cm diameter) was made on the top of the egg shell, enabling access to the CAM and evaluation of embryo viability. These windows were then sealed with transparent tape to prevent eggs dehydrating and incubated at 37 °C until day 10 of the embryonic development. At this day, ACHN cells [2×10^6 cells/egg] were collected and resuspended in 25 μL of Matrigel (BD Biosciences, San Jose, CA, USA). Following 10 min of incubation at 37 °C, ACHN cells were implanted into the CAM under sterile conditions. Three experimental groups were tested: control/vehicle (n = 12), 1.5 μM MLo1302 (n = 12) and 3 μM MLo1302 (n = 12). The shell windows were then protected again with invisible tape and the eggs returned to incubation at 37 °C until day 14 of embryonic development to allow for tumor formation. At day 14, 50 μL of the compound or vehicle were added to the tumor into the CAM, under sterile conditions, and placed again into the incubator at 37 °C after all treatments, until 72 h. Images of the CAM implants were acquired at the first day of treatment *in ovo*, prior to it, and also at 72 h after the treatment regimen, using a stereomicroscope (Olympus SZX16) attached to a digital camera SC-180 (Olympus) and CellSens imaging software (Olympus) to assess the tumor size and vascular network. After treatment, the embryos were sacrificed by incubation at − 80 °C for 10 min. Both the implants and the underlying and immediately adjacent CAM portions were cut using forceps and a small suture scissor and fixed in paraformaldehyde solution at 4% (v/v). *Ex ovo* images were then captured for each CAM implant. The excised membranes were transferred to histological cassettes, embedded in paraffin, and serially sectioned for immunohistochemical analysis. Four independent CAM assays were performed.

2.8. Global DNA methylation

Imprint® Methylated DNA Quantification kit (Sigma-Aldrich, Germany) was used to quantify 5-mC global content following manufacturer's recommendations. Briefly, after DNA extraction, using the standard phenol-chloroform method, 200 ng of total DNA were incubated with a 5-mC capture and detection antibody. Absorbance was measured using FLUOstar Omega microplate reader at 450 nm. DNA methylation levels were compared with a synthetic fully methylated DNA positive control. Three biological and three experimental replicates were performed. Calculation of the percentage of DNA global methylation was performed using the following formula: [((Mean OD sample – Mean OD blank)/(Mean OD methylated control – Mean OD blank)) × 100].

2.9. Global DNA hydroxymethylation

MethylFlash™ Global DNA Hydroxymethylation (5-hmC) ELISA Easy Kit (Epigentek) was used to quantify 5-hmC global content following manufacturer's instructions. Succinctly, 100 ng of extracted DNA was bound to strip-wells specifically treated to have a high DNA affinity. The hydroxymethylated fraction of DNA was detected using a 5-hmC mAb-based detection complex and then quantified colorimetrically by reading the absorbance in a microplate spectrophotometer. The percentage of hydroxymethylated DNA is proportional to the OD intensity measured. Three biological and three experimental replicates were performed. The percentage of hydroxymethylated DNA was calculated based on the generation of a standard curve, and then, applying the formula: [((Mean OD sample – Mean OD negative control)/(slope × amount of input sample DNA)) × 100].

2.10. DNMT3A activity

Nuclear extracts from either compound or vehicle exposed cells were obtained using the Nuclear Extract Kit (Active Motif, Rixensart, Belgium), per manufacturer's protocol. After protein quantification using Pierce BCA Protein Assay kit (Thermo Fisher Scientific), 10 μg of nuclear extract obtained from each sample was used to measure DNMT3A activity with EpiQuick™ DNMT3A Assay Kit (Epigentek, New York, USA), according to the manufacturer's instructions. Briefly, nuclear extracts from 786-O, Caki-2 and ACHN were added to a specific 96 well plate coated with CpG enriched substrate. After the enzymatic reaction, capture and detection antibodies were added to the wells. Absorbance was measured using FLUOstar Omega microplate reader, at 450 nm with background subtraction at 655 nm. Three biological and three experimental replicates were performed for each sample. The subsequent formula was used to calculate the DNMT3A activity percentage: [((Treated sample OD – Blank OD)/ (Vehicle OD – Blank OD)) × 100].

2.11. Immunohistochemistry analysis

Immunohistochemistry (IHC) on paraffin section of microtumors on CAM was performed in representative 4 μm-thick tissue sections for DNMT1, DNMT3A, DNMT3B and Ki67, using the UltraVision Detection System (Large Volume Anti-Polyvalent, HRP; Thermo Scientific Inc., USA). Briefly, deparaffinized and rehydrated slides were submitted to heat-induced antigen retrieval for 20 min at 98 °C with 10 mM citrate buffer (pH 6.0) for Ki67 and 20 min at microwave with 1 mM EDTA buffer (pH 8.0) for DNMT1, DNMT3A and DNMT3B. After endogenous peroxidase inactivation, incubation with the primary antibody was performed overnight at RT. The immune reaction was visualized with 3,3'-diamonobenzidine (Sigma-Aldrich™) as a chromogen. All sections were counterstained with Gill-2 haematoxylin and mounted with Entellan® (Merck-Millipore). A positive control was included for each antibody. The immunostaining was evaluated quantitatively using GenASIS software (Applied Spectral Imaging, ASI) using a digital camera UCMAD3 (Olympus), considering the percentage of positivity and intensity of staining. The score for immunoreactive extension was as follows: score 0: < 15% of immunoreactive cells; score 1: 15–50% of immunoreactive cells; score 2: 50–75% immunoreactive cells; score 3: > 75% of immunoreactive cells. The final score was defined as the sum of extension and intensity scores and for statistical analysis, a final score > 1 was considered positive.

2.12. Quantitative methylation-specific PCR (qMSP)

Genomic DNA extracted from cell lines using the phenol-chloroform method as previously [35] was submitted to sodium bisulfite conversion (EZ DNA Methylation-Gold™ Kit, Zymo Research, Irvine, CA, USA) following manufacturer's instructions. Sodium bisulfite modified DNA (1000 ng) was amplified by qMSP using TaqMan technology. Reactions were performed in 96-well plates using Applied Biosystems® 7500 Real-Time PCR System (Thermo Fisher Scientific). Briefly, per each well 1 μL of modified DNA, 9 μL of Master Mix using Xpert Fast Probe (uni) (GRISP, Porto, Portugal) were added. The amplification was carried out by a period of 3 min at 95 °C followed by 45 cycles with 5 s at 95 °C and 30 s at a specific temperature, depending on the primers sequence of each gene (Table A.1). Only amplifications ≤ 35 cycles were considered as positive. The PCR program was performed using Applied Biosystems® 7500 Real-Time PCR System (Thermo Fisher Scientific, Waltham, MA, USA) and all samples were run in triplicate. The methylation levels for each sample were derived from calibration curves created using serial dilutions (1:5) of bisulfite modified CpGenome™ Universal Methylated DNA. The methylation levels for each gene were calculated after normalization to *β-ACTIN*. Methyl Primer Express Software v1.0 (Applied Biosystems, Foster City, CA, USA) was used to design the

specific primers and probes.

2.13. Quantitative real-time PCR (qRT-PCR)

RNA from cultured cell lines was obtained by TRIzol method (Invitrogen, Carlsbad, CA, USA), according to manufacturer's instructions, with further complementary DNA (cDNA) synthesis using RevertAid Reverse Transcription Kit (Thermo Fisher Scientific). RNA quantification and purity were assessed in NanoDropTM Lite Spectophotometer (Cat. ND-LITE, Thermo ScientificTM). Xpert Fast Sybr (uni) blue (GRISP, Porto, Portugal) was used to quantify the expression of the target genes. The PCR program was performed using Applied Biosystems® 7500 Real-Time PCR System and consisted of 2 min at 95 °C followed by 40 cycles with 5 s at 95 °C and 30 s at a specific temperature (Table A2), and a final step of 15 s at 95 °C, 1 min at 60 °C and 30 s at 95 °C. The expression of molecular genes to assess apoptosis pathway, *CASP3* (Hs00234387_m1), cell cycle inhibition, *CDKN1A* (Hs00355782_m1), and cell proliferation, *Ki67* (Hs01032427_m1) was quantified using Taqman expression assays (purchased as pre-developed assays from Applied Biosystems) and NZYSpeedy qPCR Probe Master Mix (2 ×), ROX (NZYTech), and normalized to *GUSB* (Hs99999908_m1). The PCR program was carried out using Applied Biosystems® 7500 Real-Time PCR System and comprised a period of 2 min at 50 °C and 10 min at 95 °C followed by 40 cycles with 15 s at 95 °C and 1 min at 60 °C. The expression of each target gene was then normalized to the expression of the housekeeping (*GUSB*) gene. All the samples were run in triplicate and human reference total RNA (Agilent Technologies, USA) was used as positive control to generate a standard curve (dilutions of 1:10).

2.14. Statistical analysis

Kruskal-Wallis with post-hoc Dunn's multiple comparison test and one-way analysis of variance (ANOVA), with post-hoc Dunnet's multiple comparison test, were used to compare the results obtained in each parameter for the different compounds' concentrations and the control/vehicle, when appropriate. For immunohistochemistry analysis, the comparison of DNMT and Ki67 expressions between control/vehicle and different MLo1302 concentrations was evaluated for statistical significance using Pearson's chi square (χ^2) test. Analyses were performed with GraphPad Prism 7 (San Diego, CA, USA) and statistical significance was set at p-value < 0.05.

3. Results

3.1. MLo1302 decreases viability and increases apoptosis of RCC cell lines

The half-maximal inhibitory concentration (IC50) of cell viability by several 3-nitroflavonones synthetized in [34] was calculated for HKC8, 786-O, Caki-2 and ACHN cell lines after 72 h of compound exposure (Table 1). MLo1302 showed the lowest IC50 values for tumor cells (1.5 μM) without significantly impairing the benign cell line (HKC8) (Table 1 and Fig. 1a). MLo-1607 was used as a negative control, showing the highest IC50 values for all treated cell lines. Considering these results, IC50 and 2xIC50 values were chosen as treatment concentrations in clear cell RCC cells for 72 h to assess the effects on the RCC phenotype.

A time- and dose-dependent inhibition of RCC cell viability was observed for MLo1302. Overall, tumor cell growth suppression appeared from day 1 at both tested concentrations, with a stronger effect on day 3 with the highest dose (Fig. 1a). Indeed, 3 μM of MLo1302 induced an 83%, 91% and 86% reduction in 786-O, Caki-2 and ACHN cell viability upon 72 h of treatment, respectively. MLo1302 also increased apoptotic levels of the three tested RCC cell lines in a dose-dependent manner (Fig. 1b), particularly at the highest concentration. Importantly, it did not disclose any effect either on HKC8 cells viability with the IC50 of tumor cells (1.5 μM), nor on HKC8 apoptosis at 3 μM (HKC8 IC50 value).

Table 1
IC50 values obtained for each tested flavanone-derived compound for RCC cell lines (n = 3).

Compound	Cell Line	IC50 (μM)	Chosen Treatment Concentrations (μM)	
DD880	HKC8	9.70 ± 0.06	10	20
	786-O	4.37 ± 0.57	5	10
	Caki-2	10.26 ± 0.47	10	20
	ACHN	8.34 ± 1.31	10	20
MLo1302	HKC8	2.76 ± 0.76	3	6
	786-O	1.49 ± 0.01	1.5	3
	Caki-2	1.40 ± 0.94	1.5	3
	ACHN	1.32 ± 0.41	1.5	3
MLo1507	HKC8	16.96 ± 0.64	15	30
	786-O	13.81 ± 0.37	15	30
	Caki-2	14.99 ± 1.26	15	30
	ACHN	7.42 ± 0.03	7.5	15
MLo1508	HKC8	16.9 ± 0.59	17	34
	786-O	2.37 ± 0.01	2.5	5
	Caki-2	2.29 ± 0.29	2.5	5
	ACHN	4.84 ± 0.61	5	10
MLo1607	HKC8	104 ± 1	–	–
	786-O	108 ± 1	–	–
	Caki-2	85 ± 5	–	–
	ACHN	137 ± 1	–	–

These results were paralleled at the molecular level by the significant decrease in *Ki67* (cell proliferation marker), along with increased *CDKN1A* (negative cell cycle regulator) and *CASP3* (apoptosis marker) expression levels (Fig. 1c).

3.2. MLo1302 induces DNA damage and morphometric alterations in RCC cell lines

786-O and ACHN cells exposed to MLo1302 displayed increased cell area, higher cell granularity and nuclei heterochromatic regions comparatively to controls (Fig. 2a and Fig. S1). The latter combined with the smaller size of the cell population suggests an apoptotic status. Interestingly, cell vacuolization and debris were commonly found in cells treated with the highest MLo1302 concentrations (Figure B.1). Conversely, cell area was significantly decreased in Caki-2 cells treated with MLo1302 (Fig. 2a). Moreover, cell sphericity was significantly increased in all treated cells when compared to the respective vehicle (Fig. 2b).

RCC cell lines treated with MLo1302 increased comet tail length significantly associated with DNA damage (Fig. 3a). The same cells also disclosed increased *ATR* (serine/threonine-protein kinase), *GADD45B* (growth arrest and DNA damage 45) and *RAD9* (cell cycle checkpoint control protein) expression levels, with the exception of Caki-2 for *GADD45B* (Fig. 3b).

3.3. MLo1302 affects global DNA and histone methylation and DNMT3A activity in RCC cell lines

The pRCC cell lines (Caki-2 and ACHN) exhibited the highest basal global 5-mC content and DNMT levels compared to the ccRCC cell line 786-O (Table C1). Decreased of 5-mC content was found in all RCC cell lines upon exposure to MLo1302, with the highest reduction (55% for Caki-2% and 70% for ACHN) achieved at the lowest tested concentration (Fig. 4a). Global DNA methylation reduction associated with a significant 5-hmC global content increase in Caki-2 (44% at 1.5 μM and 62% at 3 μM) and ACHN (58% at 1.5 μM and 70% at 3 μM) cell lines (Fig. 4b). Moreover, DNMT3A activity was decreased in all RCC cell lines tested the highest reduction being achieved in Caki-2 cells (56%) exposed to 3 μM of MLo1302 (Fig. 4c). These results associated with a significant decrease of *DNMT1* and *DNMT3a* transcript levels in RCC cell lines, except for 786-O in which only *DNMT3a* was decreased after treatment (Fig. 4d). *DNMT3b,* except for Caki-2 cells, was not affected (Fig. 4d). Considering that DNA methylation is a balance between the activity of

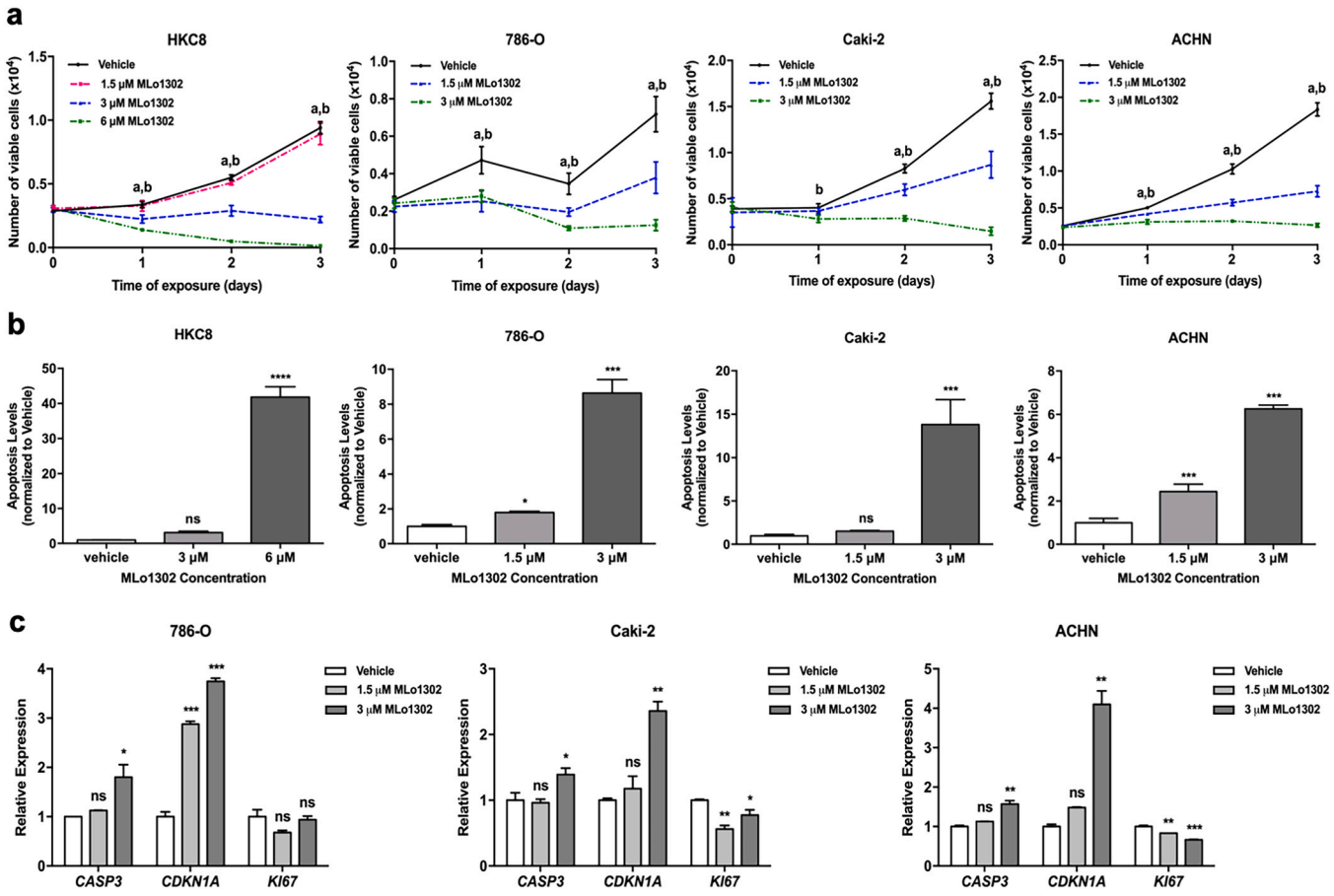

Fig. 1. MLo1302 effect on cell viability and apoptosis. (a) MLo-1302 decreased cell viability as measured by MTT assay after days 0, 1, 2 and 3, and (b) increased apoptosis levels, measured at day 3 with a phosphatidylserine-based assay, of RCC cell lines (786-O, Caki-2 and ACHN) without significantly impairing of the viability of normal cell lines (HKC8). Statistically significances were observed between (a) vehicle and at the concentration corresponding to the IC50, and (b) vehicle and at the concentration of two times the IC50. These phenotypic results were accompanied by (c) molecular analysis revealing a significant increase of *CDKN1A* (cell cycle inhibitor) and *CASP3* (marker of apoptosis pathway), and a significant decrease of *Ki67* (cell proliferation marker). All data are presented as mean of three independent experiments ± S.D., CI: 95%, based on ANOVA with post-hoc Dunnet's multiple comparison test (ns – no significant; *$p < 0.05$; **$p < 0.001$; ***$p < 0.001$; ****$p < 0.0001$).

DNMT and TET [37], we also evaluated the expression levels of the TET enzymes. *TET1* and *TET2* mRNA levels were increased in the three tested RCC cell lines, whereas *TET3* was upregulated only in ACHN cells (Fig. 4d).

3.4. MLo1302 reverses the methylation status of gene promoters in RCC cell lines

MLo1302 exposure induced demethylation (Fig. 5a) and re-expression (Fig. 5b) of the three selected RCC-related genes, *MTHFR, RASSF1A* and *TIMP3*, in Caki-2 and ACHN cell lines. In ACHN, all genes were demethylated and re-expressed at the same concentration, in particular for *RASSF1A* a 4.8-fold re-expression upon demethylation with MLo1302 was observed (Fig. 5b). 786-O cells showed a decreased of *MTHFR* promoter methylation (Fig. 5a), with no significant changes in its expression levels (Fig. 5b). In Caki-2, 3 μM of MLo1302 led to demethylation with concomitant re-expression of *MTHFR* and *TIMP3* genes. Taken together, these data indicate that MLo1302 targets DNA promoter methylation.

3.5. Anti-angiogenic effect of MLo1302 on chick embryo CAM assay

ACHN was the most responsive cell line to MLo1302, in which the greater demethylating effect was attained. Therefore, we performed CAM assay on ACHN cells treated with MLo1302. The ACHN tumor inoculated into the CAM was treated for three consecutive days to mimic the *in vitro* assays. MLo1302 effectively reduced the tumor size (Fig. 6a and b) and the number of vessels around the tumor (Fig. 6a and c). Additionally, decreased tumor proliferation by 36% and 27% for 1.5 μM and 3 μM of MLo1302, respectively, was found in the CHC group (Ki67 positive cells) compared to 58% for the control group (Fig. 6d and e), showing the anti-proliferative effect of MLo1302. Accordingly, significant decreases in DNMT1 and DNMT3A protein expression were found in the MLo1302-treated *vs* control groups (Fig. 6d and e), confirming the demethylation potential of MLo1302. DNMT3B protein was not detected in ACHN microtumors (data not shown).

4. Discussion

Deregulation of epigenetic machinery has been implicated in renal carcinogenesis and critical target genes deregulated by epigenetic mechanisms have been identified [9]. Moreover, RCC discloses a CpG island methylator phenotype (CIMP), which confers a more aggressive behavior, as observed specifically in pRCCs associated to a worse overall survival [11,38]. Finally, DNMT1, 3A and 3B proteins were found to be overexpressed in the three most frequent sporadic RCC subtypes and associated with poor prognosis [39]. Thus, DNMT inhibitors might be useful therapeutic tools for RCC. Indeed, the two nucleoside DNMTi FDA-approved for hematological neoplasi, have been tested in RCC clinical trials as monotherapy or in combination with other therapeutic

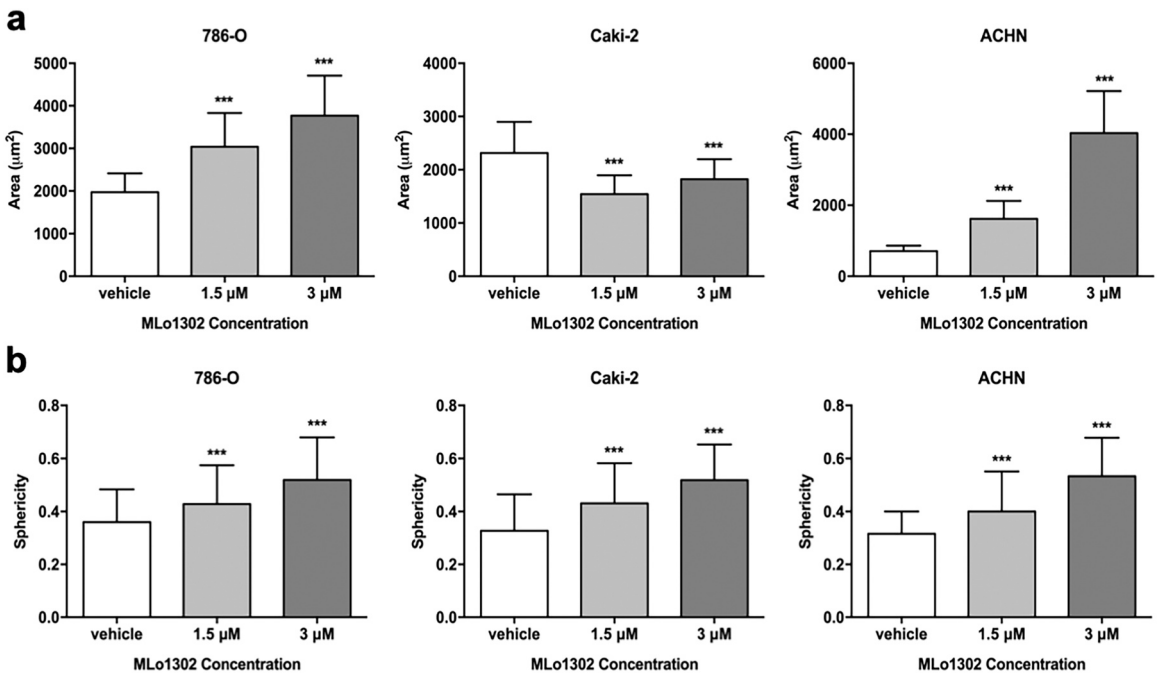

Fig. 2. MLo1302 effect on cellular morphology. MLo1302 induced morphometric alterations were followed in the three RCC cell lines by measuring the (a) cell area or (b) cell sphericity at two concentrations, the IC50 and 2xIC50. All data are presented as mean of three independent experiments ± S.D., CI: 95%, based on Kruskal-Wallis with post-hoc Dunn's multiple comparison test (ns – no significant; **p < 0.001; ***p < 0.001; ****p < 0.0001).

agents [40–43]. Nonetheless, similarly to other solid tumors, these two 5-azanucleosides showed very limited effectiveness in RCC. This might be due to limited incorporation into DNA, since solid tumors are much less proliferative compared to hematological neoplasms [44]. Thus, non-nucleoside DNMTi, which do not need to be incorporated into DNA, might overcome this constraint. Remarkably, most DNMTi developed thus far target DNMT1, whereas DNMT3A and 3B inhibition has been less explored. Although DNMT1 is the most dynamic DNMT enzyme in differentiated cells due to its role in DNA methylation mark maintenance, DNMT3A and 3B have been also considered as important targets.

Herein, we report for the first time the anti-neoplastic and demethylating activity of a newly synthetized 3-nitroflavanone DNMTi (MLo1302) in RCC cell lines. Interestingly, this compound reduced cell viability and induced apoptosis in a dose- and time-dependent manner, although it is not a potent DNMT inhibitor *in vitro* [34]. Impressively, an 83% reduction in 786-O cell viability after 72 h exposure to 3 μM of MLo1302 was observed. In comparison to 5-aza-2'-deoxycytidine, a FDA-approved nucleoside DNMTi, which reduced Caki-2 cell viability of approximately 53% and increased apoptosis 4.4-folds after 96 h of treatment at 5 μM [45], 3 μM of MLo1302 decreased Caki-2 cell viability and augmented apoptosis in a more pronounced manner after 72 h (91% and 13.8-fold, respectively). Importantly, cell viability reduction upon exposure to MLo1302 was confirmed at the molecular level through a significant decrease in *Ki67* transcript levels and increased *CDKN1A* expression. Moreover, significantly increased *CASP3* mRNA levels also corroborate the apoptosis assay results. Accordingly, in CAM assays, ACHN microtumors treated with MLo1302 showed decreased Ki67 expression, confirming the inhibitory effect upon tumor growth and angiogenesis.

MLo1302 also induced alterations in cell morphology in the three RCC cell lines. Increased cell sphericity depicted after exposure is, indeed, an epithelial phenotype marker, associated with mitigation of aggressiveness [46,47]. Importantly, this observation is in accordance with the phenotypic results of cell viability impairment and apoptosis induction. Interestingly, MLo1302 induced a dose-dependent increase in 786-O and ACHN cell area. This might be due to cell swelling, which along with debris and cell vacuolization, might suggests cell death by necrosis. Therefore, the mechanism of death in these two cell lines requires further elucidation. Conversely, treated Caki-2 cells showed significant cell area reduction that combined with heterochromatic regions, cell granularity and cellular fragmentation, suggested an apoptotic status. Importantly, cell size and sphericity increased along with decreased cell viability and cell cycle arrest. In addition, diminished *Ki67* and augmented *CDKN1A* levels might also suggest cell senescence in response to cellular stress. RCC cells also depicted marked DNA damage upon MLo1302 exposure. DNA damage was observed in a dose-dependent manner and led to ATR signaling pathway activation by *RAD9* (DNA injury sensor), *ATR* (signal transducer), and *GADD45B* overexpression, which interacts with *P21* (*CDKN1A*), culminating in cell cycle arrest and DNA repair. ATR signaling is primarily activated upon single-strand breaks (SSB), although not exclusively [48,49]. In accordance, ATR pathway activation associated with DNA repair, cell cycle arrest, apoptosis and senescence corroborate the phenotypic results. Importantly, GADD45 proteins are also known to promote active DNA demethylation of specific loci and normal gene expression, interacting with enzymes such as TET1 [50,51]. Specifically, GADD45B induces specific DNA demethylation by binding to sequence-specific transcript factors or by direct binding to nucleic acids [50,52]. Therefore, a possible mechanism of action for MLo1302 might be activation of DNA damage response (DDR) signaling pathway ATR combined to upregulation of GADD45B, which not only induces DNA repair and cell cycle arrest, but also DNA demethylation. These results might be of particularly importance, since DNA repair has been implicated in therapy-resistance [53]. Hence, the DNA repair machinery impairment induced by these compounds might be beneficial for standard cancer therapy. Moreover, DNA damage-induced phenotype might render RCC cells sensitive to poly(ADP-ribose) polymerase (PARP) inhibitors [54] and, thus, they might also be useful as chemosensitizers. Therefore, exploring combined therapies should be considered in further studies with this new and promising 3-nitroflavanone.

Interestingly, RCC cell lines exposed to MLo1302 showed a decreased in global DNA methylation at both concentrations, *i.e.* 1.5 and 3 μM, although more impressively with 1.5 μM for which a 70% reduction was achieved in ACHN and 55–60% in the other cell lines.

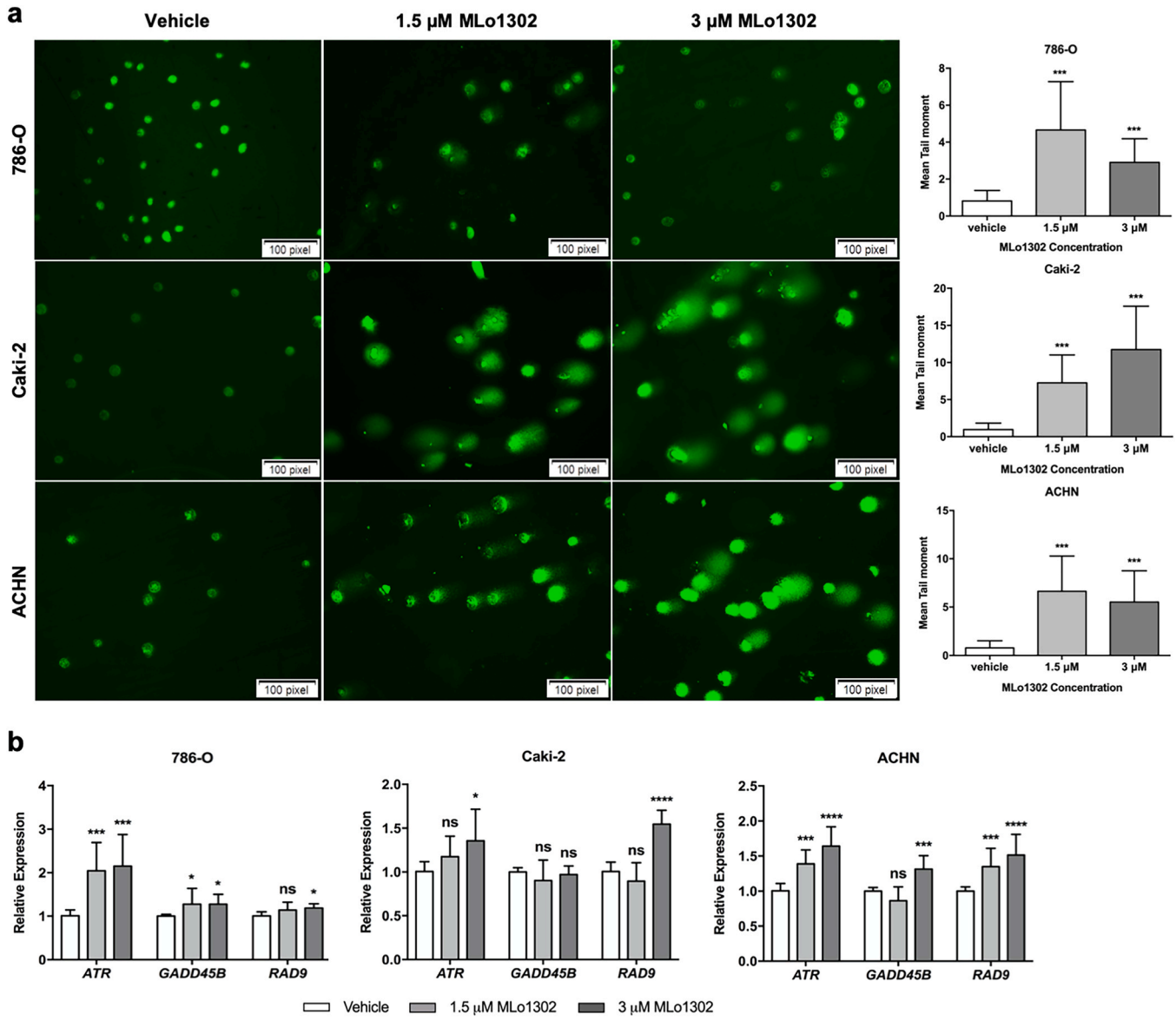

Fig. 3. MLo1302 effect on DNA damage. (a) Comet assay with mean tail moment quantification in the three cell lines at two concentrations, the IC50 and 2xIC50. Comet assay immunofluorescence images of vehicle and compounds' concentrations exposed cells counterstained with Sybr Green. Scale: 100 pixels, which is the default analysis mode of Comet Assay IV software. (b) Expression by RT qPCR of genes involved in DNA damage response signaling pathway (*ATR*, *GADD45B* and *RAD9*), in the three cell lines treated with 2 concentrations of MLo1302 All data are presented as mean of three independent experiments ± S.D., CI: 95%, based on Kruskal-Wallis with post-hoc Dunn's multiple comparison test (ns – no significant; **p < 0.001; ***p < 0.001; ****p < 0.0001).

These results are in agreement with the reported 50% reduction of the global 5-mC content observed in Caki-2 cell line treated with 1 μM 5-aza-deoxycytidine [55]. Likewise, MLo1302 showed a higher inhibitory effect on DNMT expression, especially *DNMT1* and *DNMT3a*. Remarkably, the compound led to 21–56% decrease in DNMT3A activity in all tested RCC cell lines. Furthermore, the effect of MLo1302 was also validated in an *in vivo* CAM model. The non-nucleoside MLo1302 showed an IC50 value (1.5 μM) similar to 5-aza-2'-deoxycytidine (1 μM) but displayed a more important phenotypic impact on RCC cells. To our knowledge, this is the first report of a non-nucleoside DNMT inhibitor that displays greater anti-cancer effect than 5-aza-2'-deoxycytidine in RCC cell lines.

Finally, 5-mC marks may be lost or eliminated in a passive or active manner, during DNA replication in absence of DNMT activity or through TET enzyme activity, respectively. In active DNA demethylation, 5-hmC is a product of 5-mC oxidation by the TET family proteins that, with further steps, further culminates in DNA base-excision repair (BER) pathway and replacement of a methylated cytosine by an unmodified cytosine in a replication-dependent manner [56,57]. Nonetheless, global 5-hmC loss has been reported for several tumor models [37], including RCC [58]. The 5-hmC reduction might be due to TET mutations or transcriptional/protein downregulation [59]. In our study, a significant 5-hmC increase associated with increased TET mRNA levels was found upon MLo1302 treatment, especially for *TET1*. Importantly, *TET1* was reported to be downregulated in RCC, correlating with poor prognosis [60]. In ACHN cells, *TET1* ectopic overexpression significantly associated with decreased cell viability and invasion, and increased apoptosis [60]. Overall, although the exact molecular targets of MLo1302 have not been yet identified, these data suggest that phenotypic effect of this novel compound may, at least partially, result from induced *TET1* overexpression. This leads to active DNA demethylation, along with GADD45B, as previously mentioned. Moreover, increased 5-hmC global content in Caki-2 and ACHN cell lines might contribute to the success of passive demethylation, as 5-hmC DNA may alter *in vitro* selectivity site

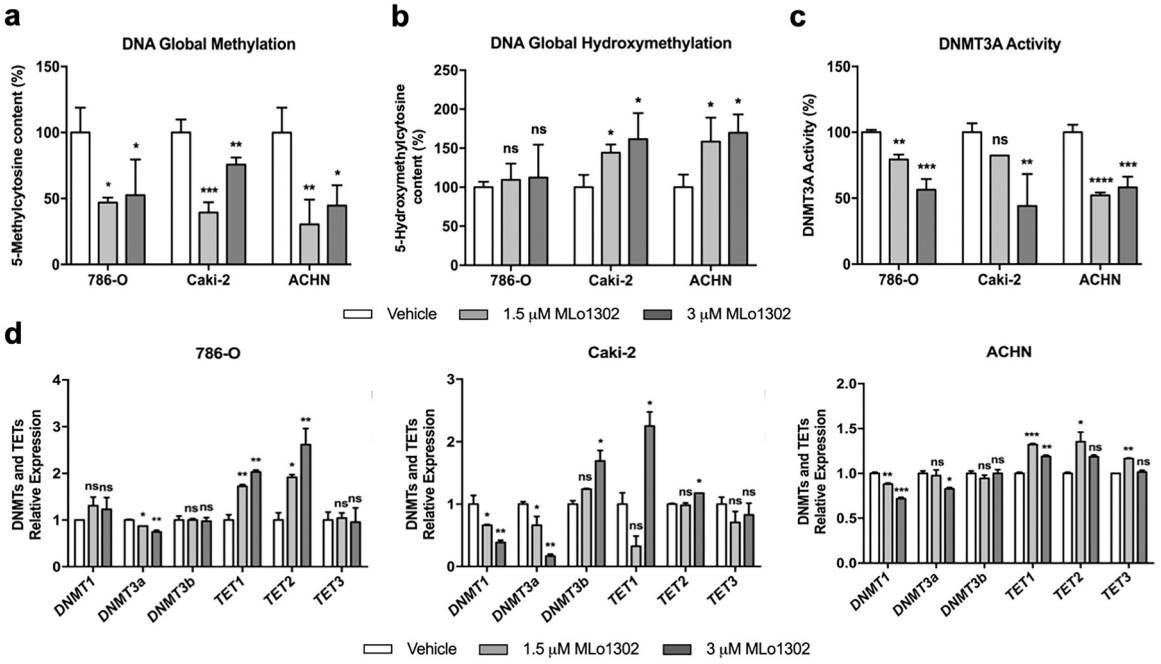

Fig. 4. MLo1302 effect on DNA methylation. MLo1302 reduced (a) DNA global methylation and increased (b) DNA global hydroxymethylation. (c) DNMT3A activity was measured in the three RCC cell lines, together with (d) *DNMT1* and *DNMT3a* mRNA levels, and *TET1* and *TET2* expression, normalized to *GUSB*. All data are presented as mean of three independent experiments ± S.D., CI: 95%, based on Kruskal-Wallis with post-hoc Dunn's multiple comparison test (ns – no significant; *p < 0.05; **p < 0.001; ***p < 0.001; ****p < 0.0001).

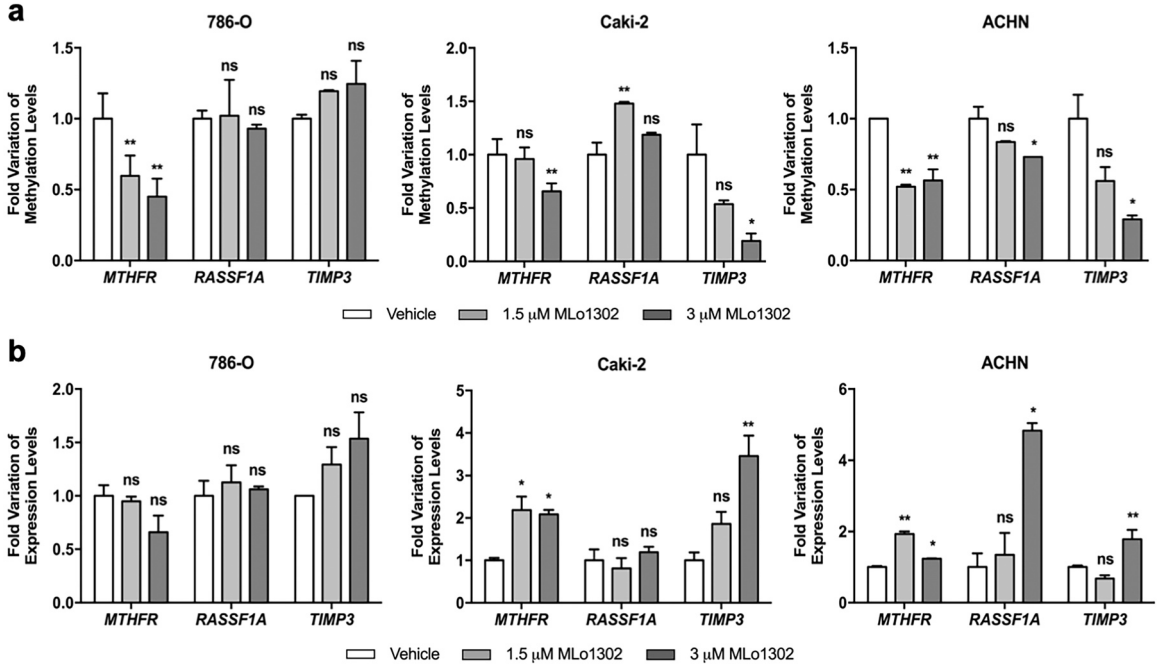

Fig. 5. MLo1302 effect on methylation and expression levels of hypermethylated genes in RCC. (a) demethylation and (b) re-expressing of *MTHFR*, *RASSF1A* and *TIMP3*, normalized to with *ACTB* and *GUSB*, were measured in all three cell lines at two concentrations, the IC50 and 2xIC50. All data are presented as mean of three independent experiments ± S.D., CI: 95%, based on Kruskal-Wallis with post-hoc Dunn's multiple comparison test (ns – no significant; *p < 0.05; **p < 0.001).

to DNMT1 and deplete its activity [61,62]. The results obtained in 786-O cells also suggest that passive DNA demethylation is involved, as no increase in global 5-hmC content or decrease in DNMT1 mRNA levels were observed. Notably, MLo1302 ability to demethylate and re-express TSGs represents a pivotal result concerning the mode of action of this compound. Specifically, *RASSF1A*, which induces cell cycle and mitotic arrest, DNA repair as well as apoptosis [63,64], is commonly silenced by hypermethylation [64], especially in pRCC [65,66]. In our study, treatment with 3 μM of MLo1302 is associated with 27% decrease in methylation and concomitant 5-fold *RASSF1A* re-expression after 3 days of exposure in ACHN cell line. Interestingly, similar results were achieved with 200 nM of 5-aza-2'-deoxycytidine after 2–6 days of treatment of ACHN cells [67]. Likewise, reduced *RASSF1A* promoter methylation and concomitant 50–100-fold re-expression was achieved in 786-O cells

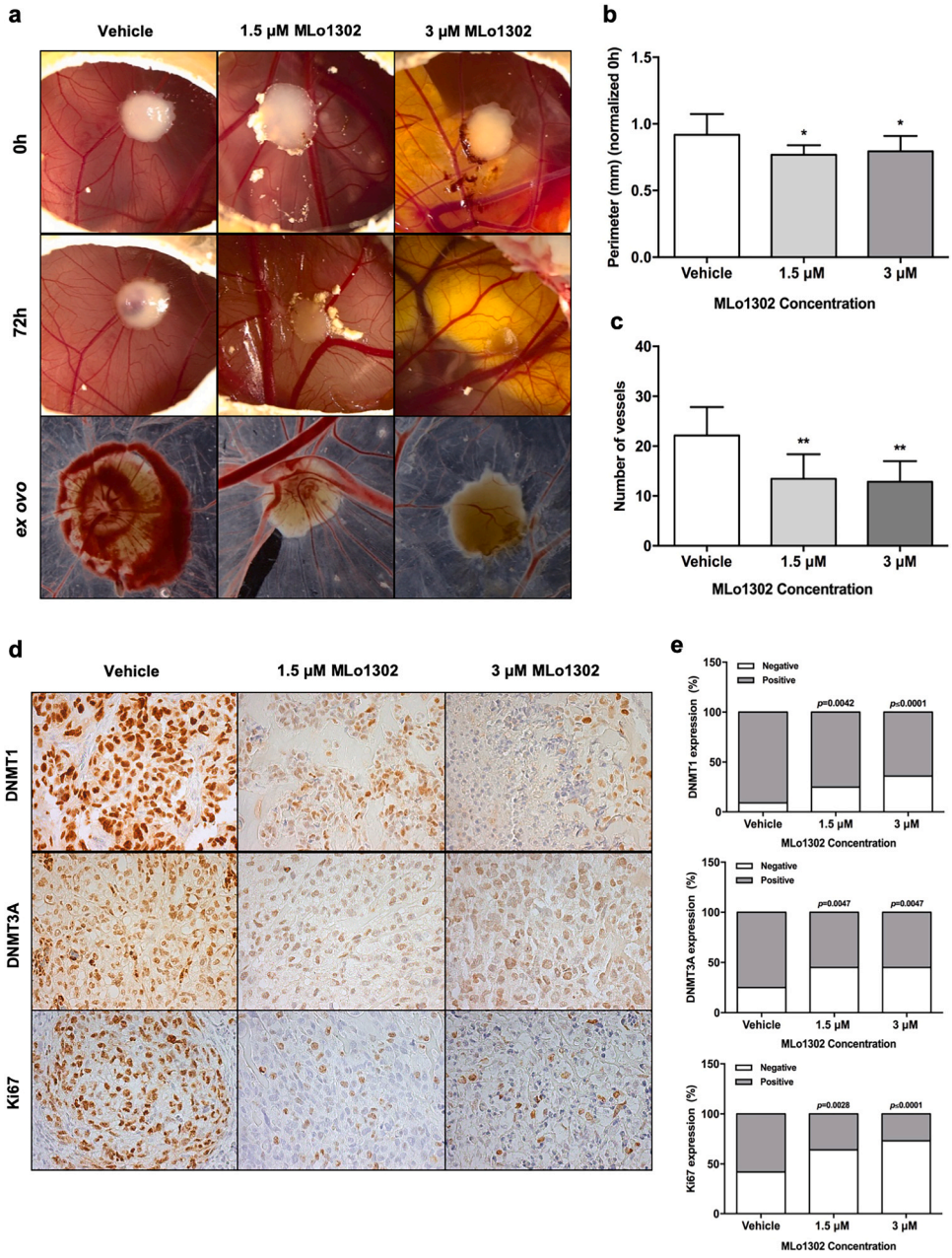

Fig. 6. MLo1302 effect on RCC growth and angiogenesis. (a) Representative pictures of ACHN microtumors *in ovo* at 0 h and 72 h after MLo1302 treatment. Tumor blood vessels recruitment in *ex ovo* pictures were also illustrated for MLo1302 treatment and respective control condition. The (b) perimeter and (c) number of blood vessels were measured in ACHN microtumors, as well as (d) nuclear DNMT1, DNMT3A and Ki67 expression by IHC and (e) their quantification in comparison with control condition. All data are presented as mean of three independent experiments ± S.D., CI: 95%, based on Kruskal-Wallis with post-hoc Dunn's multiple comparison test for the number and perimeter of blood vessels, and Pearson's chi square (χ^2) test for protein expression by immunohistochemistry (*$p < 0.05$; **$p < 0.01$).

upon exposure to 5 μM of 5-aza-2'-deoxycytidine [68]. In the same line, cells exposed to MLo1302 also displayed demethylated and re-expressed *TIMP3*, a gene encoding for a metalloproteinase inhibitor that inhibits tumor growth, invasion, migration and angiogenesis, while inducing apoptosis [69,70]. Altogether, demethylation and concomitant re-expression of these RCC-related genes further comfort the observations of the phenotypic assays.

In conclusion, MLo1302 was the most effective compound inducing phenotypic alterations in RCC cells, significantly decreasing DNA methylation at both global and gene-specific levels, entailing a less aggressive phenotype, which was also confirmed by the reduction of RCC microtumors growth and angiogenesis. Strikingly, the most impressive demethylation effects were depicted in ACHN cells, a metastatic pRCC cell line, which also disclosed the highest 5-mC basal content. Importantly, MLo1302 reduced RCC malignant features at low concentrations, which suggests clinical usefulness. As the currently available systemic therapies for mRCC are mostly based on ccRCC biology, specific therapies for pRCC and other non-ccRCC are notably lacking [71]. Pivotal clinical trials of novel therapies are carried out in ccRCC patients because it is the most commonly diagnosed RCC subtype [72], but metastatic pRCC displays similar aggressiveness [71,73], deserving due attention. Thus, the hypothesis that MLo1302 might be a new anti-neoplastic compound preferentially targeting pRCC should be considered and further explored, not only as monotherapy but also in combination with conventional or targeted therapies. Finally, to the best of our knowledge, the published data on the antineoplastic activity of non-nucleoside natural products in RCC is scarce [31,43], with only two articles reporting the anticancer properties of EGCG, but without data related to the demethylating potential [74,75]. Thus, our study might well represent the first approach to this important issue combining anti-neoplastic and demethylating properties, and render 3-nitroflavanones the focus of further investigations in RCC.

Funding

The authors would like to acknowledge the support of the Programa

Operacional Competitividade e Internacionalização (POCI), in the component FEDER, and by national funds (OE) through FCT/MCTES, in the scope of the project HyTherCaP (PTDC/MECONC/ 29030/2017) and Research Center of the Portuguese Oncology Institute of Porto (CI-IPOP-FBGEBC-27). This work was developed within the scope of the COST ACTION CM1406-Epichembio. IG was supported by COMPETE/FEDER/FCT_CI-IPOP-BPD/UID/DTP/00776/2013. POCI-01-0145-FEDER-2943 supports the junior researcher contract of VM-G.

CRediT authorship contribution statement

AM-M, IG and VM-G: Performed the experiments, drafted the manuscript, and constructed the Figures; **ML and PBA:** Synthesized the compounds; **RH, PBA and CJ**: Supervised the work and reviewed the manuscript. All authors approved the final version of the manuscript.

Declaration of Competing Interest

The authors declare that there are no conflicts of interest.

Appendix A. Supporting information

Supplementary data associated with this article can be found in the online version at doi:10.1016/j.biopha.2021.111681.

References

[1] R.L. Siegel, K.D. Miller, A. Jemal, Cancer statistics, 2016, CA Cancer J. Clin. 66 (1) (2016) 7–30.
[2] F. Bray, J. Ferlay, I. Soerjomataram, R.L. Siegel, L.A. Torre, A. Jemal, Global cancer statistics 2018: GLOBOCAN estimates of incidence and mortality worldwide for 36 cancers in 185 countries, CA Cancer J. Clin. 68 (6) (2018) 394–424.
[3] J.J. Hsieh, M.P. Purdue, S. Signoretti, C. Swanton, L. Albiges, M. Schmidinger, D. Y. Heng, J. Larkin, V. Ficarra, Renal cell carcinoma, Nat. Rev. Dis. Prim. 3 (2017) 17009.
[4] I. Duran, J. Lambea, P. Maroto, J.L. González-Larriba, L. Flores, S. Granados-Principal, M. Graupera, B. Sáez, A. Vivancos, O. Casanovas, Resistance to targeted therapies in renal cancer: the importance of changing the mechanism of action, Target. Oncol. 12 (1) (2017) 19–35.
[5] R.J. Motzer, P. Russo, Systemic therapy for renal cell carcinoma, J. Urol. 163 (2) (2000) 408–417.
[6] V.L. Costa, R. Henrique, F.R. Ribeiro, M. Pinto, J. Oliveira, F. Lobo, M.R. Teixeira, C. Jerónimo, Quantitative promoter methylation analysis of multiple cancer-related genes in renal cell tumors, BMC Cancer 7 (2007) 133.
[7] R. Henrique, A.S. Luis, C. Jeronimo, The epigenetics of renal cell tumors: from biology to biomarkers, Front. Genet. 3 (2012) 94.
[8] N. Shenoy, N. Vallumsetla, Y. Zou, J.N. Galeas, M. Shrivastava, C. Hu, K. Susztak, A. Verma, Role of DNA methylation in renal cell carcinoma, J. Hematol. Oncol. 8 (1) (2015) 88.
[9] M.R. Morris, F. Latif, The epigenetic landscape of renal cancer, Nat. Rev. Nephrol. 13 (1) (2017) 47–60.
[10] C.G.A.R. Network, Comprehensive molecular characterization of clear cell renal cell carcinoma, Nature 499 (7456) (2013) 43–49.
[11] C.G.A.R. Network, Comprehensive molecular characterization of papillary renal-cell carcinoma, N. Engl. J. Med. 374 (2) (2016) 135–145.
[12] T. Ushijima, K. Asada, Aberrant DNA methylation in contrast with mutations, Cancer Sci. 101 (2) (2010) 300–305.
[13] L. Lopez-Serra, M. Esteller, Proteins that bind methylated DNA and human cancer: reading the wrong words, Br. J. Cancer 98 (12) (2008) 1881–1885.
[14] M. Lopez, L. Halby, P.B. Arimondo, DNA methyltransferase inhibitors: development and applications, Adv. Exp. Med. Biol. 945 (2016) 431–473.
[15] M. Lopez, et al., Drug discovery methods. Drug Discovery in Cancer Epigenetics, Elsevier, 2016, pp. 63–95.
[16] K. Ghoshal, J. Datta, S. Majumder, S. Bai, H. Kutay, T. Motiwala, S.T. Jacob, 5-Aza-deoxycytidine induces selective degradation of DNA methyltransferase 1 by a proteasomal pathway that requires the KEN box, bromo-adjacent homology domain, and nuclear localization signal, Mol. Cell. Biol. 25 (11) (2005) 4727–4741.
[17] T.K. Kelly, D.D. De Carvalho, P.A. Jones, Epigenetic modifications as therapeutic targets, Nat. Biotechnol. 28 (10) (2010) 1069–1078.
[18] D. Dhanak, P. Jackson, Development and classes of epigenetic drugs for cancer, Biochem. Biophys. Res. Commun. 455 (1–2) (2014) 58–69.
[19] P. Wijermans, M. Lübbert, G. Verhoef, A. Bosly, C. Ravoet, M. Andre, A. Ferrant, Low-dose 5-aza-2'-deoxycytidine, a DNA hypomethylating agent, for the treatment of high-risk myelodysplastic syndrome: a multicenter phase II study in elderly patients, J. Clin. Oncol. Off. J. Am. Soc. Clin. Oncol. 18 (5) (2000) 956–962, 956-956.
[20] J.P. Issa, G. Garcia-Manero, F.J. Giles, R. Mannari, D. Thomas, S. Faderl, E. Bayar, J. Lyons, C.S. Rosenfeld, J. Cortes, H.M. Kantarjian, Phase 1 study of low-dose prolonged exposure schedules of the hypomethylating agent 5-aza-2′-deoxycytidine (decitabine) in hematopoietic malignancies, Blood 103 (5) (2004) 1635–1640.
[21] E. Kaminskas, A. Farrell, S. Abraham, A. Baird, L.S. Hsieh, S.L. Lee, J.K. Leighton, H. Patel, A. Rahman, R. Sridhara, Y.C. Wang, R. Pazdur, FDA, Approval summary: azacitidine for treatment of myelodysplastic syndrome subtypes, Clin. Cancer Res. 11 (10) (2005) 3604–3608.
[22] H. Kantarjian, J.P. Issa, C.S. Rosenfeld, J.M. Bennett, M. Albitar, J. DiPersio, V. Klimek, J. Slack, C. de Castro, F. Ravandi, R. Helmer, L. Shen, S.D. Nimer, R. Leavitt, A. Raza, H. Saba, Decitabine improves patient outcomes in myelodysplastic syndromes, Cancer 106 (8) (2006) 1794–1803.
[23] F. Braiteh, A.O. Soriano, G. Garcia-Manero, D. Hong, M.M. Johnson, P. Silva Lde, H. Yang, S. Alexander, J. Wolff, R. Kurzrock, Phase I study of epigenetic modulation with 5-azacytidine and valproic acid in patients with advanced cancers, Clin. Cancer Res. 14 (19) (2008) 6296–6301.
[24] B.A. Chabner, J.C. Drake, D.G. Johns, Deamination of 5-azacytidine by a human leukemia cell cytidine deaminase, Biochem. Pharmacol. 22 (21) (1973) 2763–2765.
[25] J. Laliberte, V.E. Marquez, R.L. Momparler, Potent inhibitors for the deamination of cytosine arabinoside and 5-aza-2′-deoxycytidine by human cytidine deaminase, Cancer Chemother. Pharmacol. 30 (1) (1992) 7–11.
[26] J. Worm, P. Guldberg, DNA methylation: an epigenetic pathway to cancer and a promising target for anticancer therapy, J. Oral. Pathol. Med. 31 (8) (2002) 443–449.
[27] D.V. Santi, A. Norment, C.E. Garrett, Covalent bond formation between a DNA-cytosine methyltransferase and DNA containing 5-azacytosine, Proc. Natl. Acad. Sci. 81 (22) (1984) 6993–6997.
[28] B. Brueckner, F. Lyko, DNA methyltransferase inhibitors: old and new drugs for an epigenetic cancer therapy, Trends Pharmacol. Sci. 25 (11) (2004) 551–554.
[29] R. Aggarwal, M. Jha, A. Shrivastava, A.K. Jha, Natural compounds: role in reversal of epigenetic changes, Biochemistry Mosc. 80 (8) (2015) 972–989.
[30] S. Lascano, M. Lopez, P.B. Arimondo, Natural products and chemical biology tools: alternatives to target epigenetic mechanisms in cancers, Chem. Rec. 18 (12) (2018) 1854–1876.
[31] Y. Zhou, J. Zheng, Y. Li, D.P. Xu, S. Li, Y.M. Chen, H.B. Li, Natural polyphenols for prevention and treatment of cancer, Nutrients 8 (8) (2016) 515.
[32] C. Manach, A. Scalbert, C. Morand, C. Rémésy, L. Jiménez, Polyphenols: food sources and bioavailability, Am. J. Clin. Nutr. 79 (5) (2004) 727–747.
[33] M. Fang, D. Chen, C.S. Yang, Dietary polyphenols may affect DNA methylation, J. Nutr. 137 (1) (2007) 223S–228S.
[34] D. Pechalrieu, D. Dauzonne, P.B. Arimondo, M. Lopez, Synthesis of novel 3-halo-3-nitroflavanones and their activities as DNA methyltransferase inhibitors in cancer cells, Eur. J. Med Chem. 186 (2020), 111829.
[35] I. Graça, E.J. Sousa, P. Costa-Pinheiro, F.Q. Vieira, J. Torres-Ferreira, M.G. Martins, R. Henrique, C. Jerónimo, Anti-neoplastic properties of hydralazine in prostate cancer, Oncotarget 5 (15) (2014) 5950–5964.
[36] P.L. Olive, J.P. Banáth, The comet assay: a method to measure DNA damage in individual cells, Nat. Protoc. 1 (1) (2006) 23–29.
[37] J.P. Thomson, R.R. Meehan, The application of genome-wide 5-hydroxymethylcytosine studies in cancer research, Epigenomics 9 (1) (2017) 77–91.
[38] E. Arai, S. Chiku, T. Mori, M. Gotoh, T. Nakagawa, H. Fujimoto, Y. Kanai, Single-CpG-resolution methylome analysis identifies clinicopathologically aggressive CpG island methylator phenotype clear cell renal cell carcinomas, Carcinogenesis 33 (8) (2012) 1487–1493.
[39] M. Li, Y. Wang, Y. Song, R. Bu, B. Yin, X. Fei, Q. Guo, B. Wu, Expression profiling and clinicopathological significance of DNA methyltransferase 1, 3A and 3B in sporadic human renal cell carcinoma, Int. J. Clin. Exp. Pathol. 7 (11) (2014) 7597–7609.
[40] D.J. Stewart, J.P. Issa, R. Kurzrock, M.I. Nunez, J. Jelinek, D. Hong, Y. Oki, Z. Guo, S. Gupta, I.I. Wistuba, Decitabine effect on tumor global DNA methylation and other parameters in a phase I trial in refractory solid tumors and lymphomas, Clin. Cancer Res. 15 (11) (2009) 3881–3888.
[41] J.A. Gollob, C.J. Sciambi, B.L. Peterson, T. Richmond, M. Thoreson, K. Moran, H. K. Dressman, J. Jelinek, J.P. Issa, Phase I trial of sequential low-dose 5-aza-2′-deoxycytidine plus high-dose intravenous bolus interleukin-2 in patients with melanoma or renal cell carcinoma, Clin. Cancer Res. 12 (15) (2006) 4619–4627.
[42] J. Lin, J. Gilbert, M.A. Rudek, J.A. Zwiebel, S. Gore, A. Jiemjit, M. Zhao, S. D. Baker, R.F. Ambinder, J.G. Herman, R.C. Donehower, M.A. Carducci, A phase I dose-finding study of 5-azacytidine in combination with sodium phenylbutyrate in patients with refractory solid tumors, Clin. Cancer Res. 15 (19) (2009) 6241–6249.
[43] Â. Marques-Magalhães, I. Graça, R. Henrique, C. Jerónimo, Targeting DNA methyltranferases in urological tumors, Front. Pharmacol. 9 (2018) 366.
[44] J.S. Graham, S.B. Kaye, R. Brown, The promises and pitfalls of epigenetic therapies in solid tumours, Eur. J. Cancer 45 (7) (2009) 1129–1136.
[45] E. Konac, N. Varol, A. Yilmaz, S. Menevse, S. Sozen, DNA methyltransferase inhibitor-mediated apoptosis in the Wnt/β-catenin signal pathway in a renal cell carcinoma cell line, Exp. Biol. Med. 238 (9) (2013) 1009–1016.
[46] S.E. Leggett, J.Y. Sim, J.E. Rubins, Z.J. Neronha, E.K. Williams, I.Y. Wong, Morphological single cell profiling of the epithelial–mesenchymal transition, Integr. Biol. 8 (11) (2016) 1133–1144.
[47] S.D. Bhattacharya, Z. Mi, L.J. Talbot, H. Guo, P.C. Kuo, Human mesenchymal stem cell and epithelial hepatic carcinoma cell lines in admixture: concurrent stimulation of cancer-associated fibroblasts and epithelial-to-mesenchymal transition markers, Surgery 152 (3) (2012) 449–454.
[48] A. Marechal, L. Zou, DNA damage sensing by the ATM and ATR kinases, Cold Spring Harb. Perspect. Biol. 5 (2013) 9.

[49] L. Zou, S.J. Elledge, Sensing DNA damage through ATRIP recognition of RPA-ssDNA complexes, Science 300 (5625) (2003) 1542–1548.
[50] D.K. Ma, J.U. Guo, G.L. Ming, H. Song, DNA excision repair proteins and Gadd45 as molecular players for active DNA demethylation, Cell Cycle 8 (10) (2009) 1526–1531.
[51] K.M. Schüle, M. Leichsenring, T. Andreani, V. Vastolo, M. Mallick, M.U. Musheev, E. Karaulanov, C. Niehrs, GADD45 promotes locus-specific DNA demethylation and 2C cycling in embryonic stem cells, Genes Dev. 33 (13–14) (2019) 782–798.
[52] Y.W. Yi, D. Kim, N. Jung, S.S. Hong, H.S. Lee, I. Bae, Gadd45 family proteins are coactivators of nuclear hormone receptors, Biochem Biophys. Res Commun. 272 (1) (2000) 193–198.
[53] S.P. Jackson, J. Bartek, The DNA-damage response in human biology and disease, Nature 461 (7267) (2009) 1071–1078.
[54] A. Okazaki, P.A. Gameiro, D. Christodoulou, L. Laviollette, M. Schneider, F. Chaves, A. Stemmer-Rachamimov, S.A. Yazinski, R. Lee, G. Stephanopoulos, L. Zou, O. Iliopoulos, Glutaminase and poly (ADP-ribose) polymerase inhibitors suppress pyrimidine synthesis and VHL-deficient renal cancers, J. Clin. Investig. 127 (5) (2017) 1631–1645.
[55] S. Winter, P. Fisel, F. Büttner, S. Rausch, D. D'Amico, J. Hennenlotter, S. Kruck, A. T. Nies, A. Stenzl, K. Junker, M. Scharpf, U. Hofmann, H. van der Kuip, F. Fend, G. Ott, A. Agaimy, A. Hartmann, J. Bedke, M. Schwab, E. Schaeffeler, Methylomes of renal cell lines and tumors or metastases differ significantly with impact on pharmacogenes, Sci. Rep. 6 (2016) 29930.
[56] M. Bochtler, A. Kolano, G.L. Xu, DNA demethylation pathways: additional players and regulators, Bioessays 39 (1) (2017) 1–13.
[57] D.-Q. Shi, I. Ali, J. Tang, W.C. Yang, New insights into 5hmC DNA modification: generation, distribution and function, Front. Genet. 8 (2017), 100-100.
[58] K. Chen, J. Zhang, Z. Guo, Q. Ma, Z. Xu, Y. Zhou, Z. Xu, Z. Li, Y. Liu, X. Ye, X. Li, B. Yuan, Y. Ke, C. He, L. Zhou, J. Liu, W. Ci, Loss of 5-hydroxymethylcytosine is linked to gene body hypermethylation in kidney cancer, Cell Res. 26 (1) (2016) 103–118.
[59] K.D. Rasmussen, K. Helin, Role of TET enzymes in DNA methylation, development, and cancer, Genes Dev. 30 (7) (2016) 733–750.
[60] M. Fan, X. He, X. Xu, Restored expression levels of TET1 decrease the proliferation and migration of renal carcinoma cells, Mol. Med. Rep. 12 (4) (2015) 4837–4842.
[61] V. Valinluck, L.C. Sowers, Endogenous cytosine damage products alter the site selectivity of human DNA maintenance methyltransferase DNMT1, Cancer Res. 67 (3) (2007) 946–950.
[62] D. Ji, K. Lin, J. Song, Y. Wang, Effects of Tet-induced oxidation products of 5-methylcytosine on Dnmt1- and DNMT3a-mediated cytosine methylation, Mol. Biosyst. 10 (7) (2014) 1749–1752.
[63] G. Malpeli, G. Innamorati, I. Decimo, M. Bencivenga, A.H. Nwabo Kamdje, R. Perris, C. Bassi, Methylation dynamics of RASSF1A and its impact on cancer, Cancers Basel 11 (7) (2019).
[64] H. Donninger, M.D. Vos, G.J. Clark, The RASSF1A tumor suppressor, J. Cell Sci. 120 (18) (2007) 3163–3172.
[65] V.L. Costa, R. Henrique, F.R. Ribeiro, M. Pinto, J. Oliveira, F. Lobo, M.R. Teixeira, C. Jerónimo, Quantitative promoter methylation analysis of multiple cancer-related genes in renal cell tumors, BMC Cancer 7 (1) (2007) 133.
[66] M.R. Morris, E.R. Maher, Epigenetics of renal cell carcinoma: the path towards new diagnostics and therapeutics, Genome Med. 2 (9) (2010) 59.
[67] F.J. Reu, D.W. Leaman, R.R. Maitra, S.I. Bae, L. Cherkassky, M.W. Fox, D. R. Rempinski, N. Beaulieu, A.R. MacLeod, E.C. Borden, Expression of RASSF1A, an epigenetically silenced tumor suppressor, overcomes resistance to apoptosis induction by interferons, Cancer Res. 66 (5) (2006) 2785–2793.
[68] K. Dreijerink, et al., The candidate tumor suppressor gene, RASSF1A, from human chromosome 3p21. 3 is involved in kidney tumorigenesis, Proc. Natl. Acad. Sci. 98 (13) (2001) 7504–7509.
[69] J.H. Qi, Q. Ebrahem, N. Moore, G. Murphy, L. Claesson-Welsh, M. Bond, A. Baker, B. Anand-Apte, A novel function for tissue inhibitor of metalloproteinases-3 (TIMP3): inhibition of angiogenesis by blockage of VEGF binding to VEGF receptor-2, Nat. Med. 9 (4) (2003) 407–415.
[70] A.H. Baker, D.R. Edwards, G. Murphy, Metalloproteinase inhibitors: biological actions and therapeutic opportunities, J. Cell Sci. 115 (Pt 19) (2002) 3719–3727.
[71] B. Escudier, C. Porta, M. Schmidinger, N. Rioux-Leclercq, A. Bex, V. Khoo, V. Gruenvald, A. Horwich, C. ESMO Guidelines, Renal cell carcinoma: ESMO clinical practice guidelines for diagnosis, treatment and follow-up, Ann. Oncol. 27 (Suppl_5) (2016) v58–v68.
[72] A. Sánchez-Gastaldo, E. Kempf, A. González Del Alba, I. Duran, Systemic treatment of renal cell cancer: a comprehensive review, Cancer Treat. Rev. 60 (2017) 77–89.
[73] Ulbright T., A.M., Balzer B et al., WHO Classification of of Tumours of the Urinary System and Male Genital Organs. 2016.
[74] M. Carvalho, C. Jerónimo, P. Valentão, P.B. Andrade, B.M. Silva, Green tea: a promising anticancer agent for renal cell carcinoma, Food Chem. 122 (1) (2010) 49–54.
[75] S.-J. Chen, X.D. Yao, B.O. Peng, Y.F. Xu, G.C. Wang, J. Huang, M. Liu, J.H. Zheng, Epigallocatechin-3-gallate inhibits migration and invasion of human renal carcinoma cells by downregulating matrix metalloproteinase-2 and matrix metalloproteinase-9, Exp. Ther. Med. 11 (4) (2016) 1243–1248.